Observation of an intrinsic bandgap and Landau level renormalization in graphene/boron-nitride heterostructures

Zhi-Guo Chen[1], Zhiwen Shi[2], Wei Yang[3], Xiaobo Lu[3], You Lai[1], Hugen Yan[4], Feng Wang[2,5], Guangyu Zhang[3] & Zhiqiang Li[1]

Van der Waals heterostructures formed by assembling different two-dimensional atomic crystals into stacks can lead to many new phenomena and device functionalities. In particular, graphene/boron-nitride heterostructures have emerged as a very promising system for band engineering of graphene. However, the intrinsic value and origin of the bandgap in such heterostructures remain unresolved. Here we report the observation of an intrinsic bandgap in epitaxial graphene/boron-nitride heterostructures with zero crystallographic alignment angle. Magneto-optical spectroscopy provides a direct probe of the Landau level transitions in this system and reveals a bandgap of ~ 38 meV (440 K). Moreover, the Landau level transitions are characterized by effective Fermi velocities with a critical dependence on specific transitions and magnetic field. These findings highlight the important role of many-body interactions in determining the fundamental properties of graphene heterostructures.

[1] National High Magnetic Field Laboratory, Tallahassee, Florida 32310, USA. [2] Department of Physics, University of California at Berkeley, Berkeley, California 94720, USA. [3] Beijing National Laboratory for Condensed Matter Physics and Institute of Physics, Chinese Academy of Sciences, Beijing 100190, China. [4] IBM Thomas J. Watson Research Center, Yorktown Heights, New York 10598, USA. [5] Materials Science Division, Lawrence Berkeley National Laboratory, Berkeley, California 94720, USA. Correspondence and requests for materials should be addressed to Z.L. (email: zli@magnet.fsu.edu) or to G.Z. (email: gyzhang@iphy.ac.cn) or to F.W. (email: fengwang76@berkeley.edu).

Heterostructures consisting of two-dimensional (2D) layers of graphene, hexagonal boron-nitride (h-BN), MoS$_2$ and so on coupled by van der Waals interactions[1,2] exhibit many intriguing physical properties[2] and new device functionalities that are not achievable by individual constituting materials[3–7]. In particular, graphene/h-BN heterostructures have shown great potentials for band structure engineering of graphene[8–20] including inducing a bandgap[11,13,15–20] (Fig. 1a), which is of great fundamental[21–24] and technological[25] interest. The coupling between graphene and h-BN results in a periodic moiré superlattice potential due to a 1.8% lattice mismatch[8], which gives rise to superlattice minibands and new Dirac points near the edges of the superlattice Brillouin zone[8–12,14]. Furthermore, the local sublattice symmetry of graphene is broken owing to different local potentials produced by boron and nitrogen atoms[17–19] (Fig. 1b), inducing a local bandgap[18,19]. Although this effect varies spatially and is predicted to nearly disappear after spatial averaging[18], transport studies showed signatures of a global bandgap in these heterostructures[11,13]. It is suggested that many-body interactions may be responsible for the observed bandgap[15,16], but the issue remains unresolved experimentally.

Here we report the observation of a finite bandgap in epitaxially grown graphene/h-BN heterostructures with zero crystallographic rotation angle[12] (Fig. 1c; see Methods section) by probing their Landau levels (LL) using magneto-optical spectroscopy. The inter-band (inter-LL) transition peaks measured by optical spectroscopy are determined by peaks in the joint density of states between two bands (LLs), which are not limited by disorder[26,27] such as impurities and defects, and therefore enable the measurement of the intrinsic bandgap. On the other hand, disorder may lead to a reduced mobility gap (or thermal activation gap) measured by other techniques compared with the intrinsic gap[26,27].

At zero magnetic field, the energy dispersion of graphene with a bandgap Δ is[11,28] $E(p) = \pm \sqrt{v_F^2 p^2 + (\Delta/2)^2}$, where v_F is the Fermi velocity and p is the momentum (Fig. 1a). In a magnetic field, B, the electronic spectrum of pristine graphene is quantized into LLs described by refs 11,28:

$$E_n = \text{sgn}(n)\sqrt{2e\hbar v_F^2 B|n|}, \qquad (1)$$

where e is the elementary charge, $\hbar$ is Planck's constant divided by 2π, the integer n is LL index, and $\text{sgn}(n)$ is the sign function. The LLs for gapped graphene have the form[28]:

$$E_n = \pm(\Delta/2)\delta_{n,0} + \text{sgn}(n)\sqrt{2e\hbar v_F^2 B|n| + (\Delta/2)^2}, \qquad (2)$$

which features two zeroth LLs labelled as $n = +0$ and $n = -0$ with energies of $E_{\pm 0} = \pm\Delta/2$. Here δ is the Kronecker delta function. Therefore, the bandgap of graphene can be explored by probing its LL energy spectrum.

Our study provides a direct spectroscopic determination of the bandgap in epitaxial graphene/h-BN heterostructures from optical measurements of LL transitions. We observe an intrinsic bandgap of ~ 38 meV (440 K) in this system, which is comparable to the gap value found in transport studies[11,13]. Moreover, we find different values of effective Fermi velocity for different LL transitions, indicating LL renormalization by interaction effects. These findings have broad implications for the fundamental understanding of graphene heterostructures and their potential applications.

Results

Transmission spectra in magnetic field. Infrared (IR) transmission spectra $T(B)$ were measured in magnetic field applied perpendicular to the samples as shown in Fig. 1d (see Methods section). Figure 2 depicts the $T(B)/T(B_0)$ spectra for a
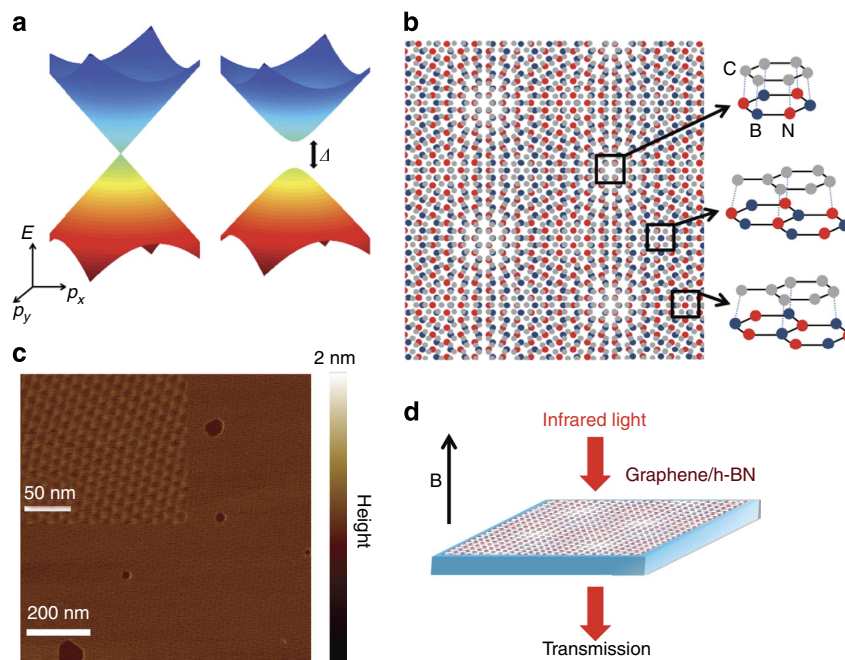

Figure 1 | Graphene/h-BN heterostructures. (**a**) Energy spectrum of pristine graphene (left) and gapped graphene (right). (**b**) Schematic of the moire pattern in graphene on h-BN with zero crystallographic rotation angle and an exaggerated lattice mismatch of 11% (carbon, grey; boron, blue; and nitrogen, red). The lattice alignments in different regions lead to different local sublattice symmetry breaking in graphene. (**c**) Atomic force microscopy image of a monolayer graphene sample grown on h-BN and treated by hydrogen plasma etching, with bare BN shown in dark colour. The inset shows the observed moiré pattern with a periodicity of 15 ± 1 nm. (**d**) Schematic of the magneto-optical measurements.
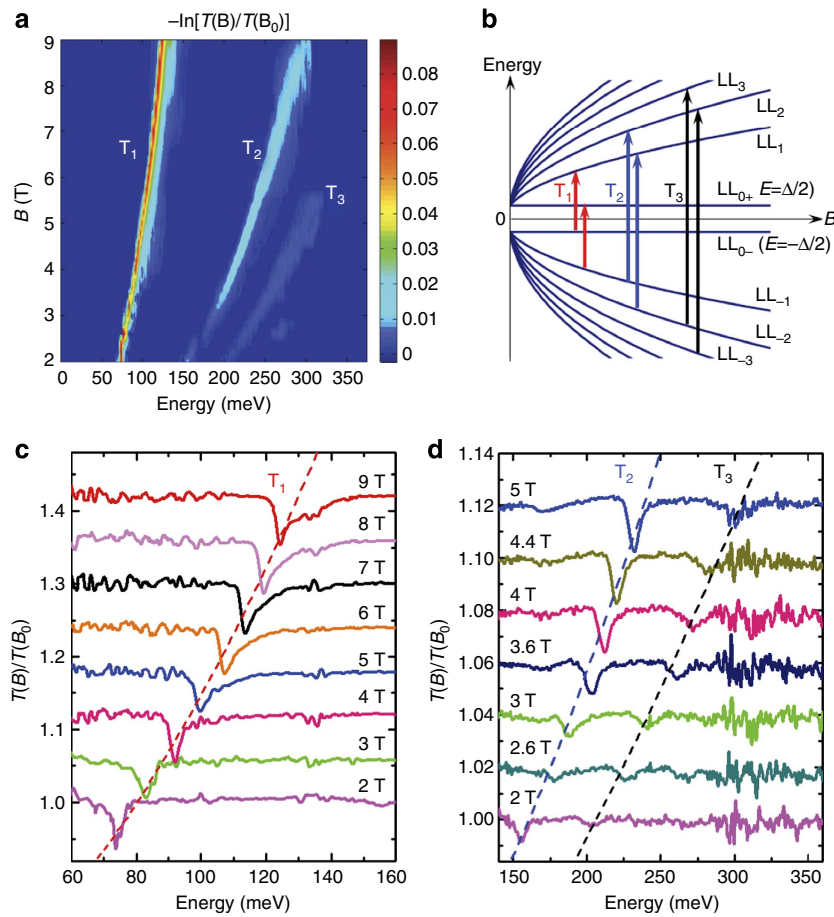
Figure 2 | Magneto-transmission ratio spectra of graphene/h-BN. (**a**) Colour rendition of the $-\ln[T(B)/T(B_0)]$ spectra as a function of magnetic field and energy for sample 1, where $B_0 = 0$ T. (**b**) Schematic of LLs of gapped graphene. The arrows indicate transitions observed in this study. (**c,d**) Several representative $T(B)/T(B_0)$ spectra for sample 1; dashed lines are guides to eyes. For clarity, the data in **c** and **d** are displaced from one another by 0.06 and 0.02, respectively.

representative sample, where $B_0 = 0$ T. Data for more samples are shown in Supplementary Fig. 1. Three dip features denoted as T_1, T_2 and T_3 are observed, all of which systematically shift to higher energies with increasing magnetic field. The zero-field transmission spectrum $T(B_0)$ of either pristine or gapped graphene shows a step-like feature without any sharp resonances in the energy range explored here, so the observed dip features in the $T(B)/T(B_0)$ spectra are corresponding to transmission minima in $T(B)$ and thus absorption peaks in magnetic fields (Supplementary Fig. 2 and Supplementary Note 1).

The effective bulk mobility of our samples estimated from the widths of the resonances in the optical spectra is higher than $50,000 \, \text{cm}^2 \, \text{V}^{-1} \, \text{s}^{-1}$ (Supplementary Fig. 3 and Supplementary Note 2). Our optical data also indicate that the Fermi energy for our samples is in the range of $E_F < 19$ meV (Supplementary Note 3).

Observed LL transitions. The energies (E) of all observed features in graphene/h-BN exhibit an approximate linear dependence on $\sqrt{B}$ (or equivalently, E^2 has an approximate linear dependence on B) in our spectral range as shown in Fig. 3. However, they all show non-zero energy intercepts at zero magnetic field under linear extrapolations, in stark contrast to the LL transitions of pristine graphene described by equation (1), which converge to zero energy at zero field[29,30]. Similar behaviours were observed in all five samples we have

measured (Supplementary Fig. 1). Within the non-interacting single-particle picture, the finite zero-field extrapolation values of all observed absorption energies suggest that the LLs of our graphene/h-BN samples are described by equation (2). From the selection rule[31] for allowed optical transitions from LL_n to $LL_{n'}$, $\Delta n = |n| - |n'| = \pm 1$, and a quantitative comparison with equation (2), we assign feature T_1 to transitions of $LL_{-1} \rightarrow LL_{+0}$ and $LL_{-0} \rightarrow LL_{+1}$ (Fig. 2b), with an energy given by:

$$E_{T_1} = \sqrt{2e\hbar v_F^2 B + (\Delta/2)^2} + \Delta/2 \qquad (3)$$

Fitting the T_1 feature based on equation (3) from a least squares fit yields a bandgap $\Delta \approx 38 \pm 4$ meV and an effective Fermi velocity $v_F^{T_1} \approx (0.96 \pm 0.02) \times 10^6 \, \text{m s}^{-1}$ (Supplementary Table 1 and Supplementary Note 4). We emphasize that the bandgap explored here is at the main Dirac point of graphene instead of the secondary Dirac points at the edges of graphene/BN superlattice Brillouin zone[8–12]. The T_1 transition energies in Fig. 2 are well below the energy (~ 200 meV) of the secondary Dirac points[9–12], so the LLs in this energy region are not significantly affected by the strong band structure modifications at the boundary of the superlattice Brillouin zone, which is supported by the observed linear $\sqrt{B}$ dependence of the LL transition energy.

The observed T_2 and T_3 features have higher energies compared with T_1 features and can be assigned as (Fig. 2b):
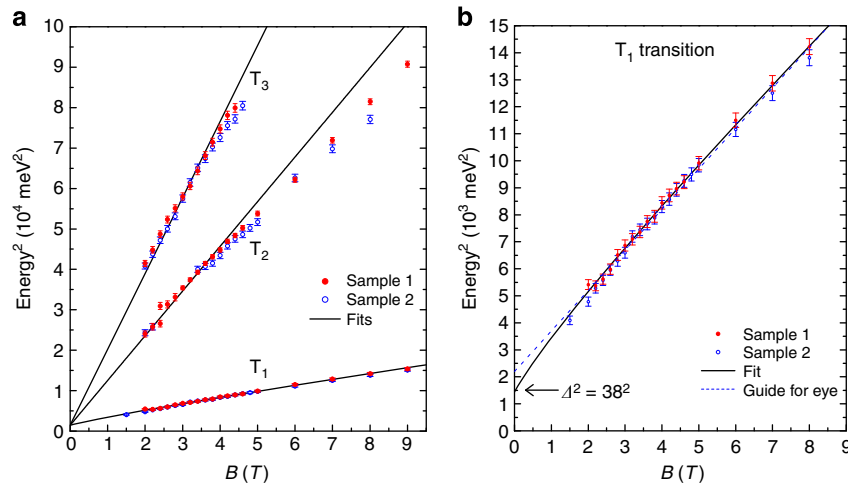
Figure 3 | LL transition energies of graphene/h-BN. (**a**) All observed transitions shown in a E^2–B plot. Symbols: data for sample 1 and 2. Solid lines: best fits to the data for sample 1 using equations (3)–(5) and parameters discussed in the text. $\Delta = 38$ meV and $v_F^{T_3} \approx 1.20 \times 10^6$ m s^{-1} are used for the fit to T_3 transition shown here. (**b**) The low energy part of **a** to highlight the extraction of the gap. Dashed line: a guide for eye showing linear extrapolation of the data. The error bars in both panels, $\delta(E^2)$, are calculated as $\delta(E^2) = 2E\delta(E)$, where $\delta(E)$ is the uncertainty in determining the energy of each LL transition from the $T(B)/T(B_0)$ spectra.
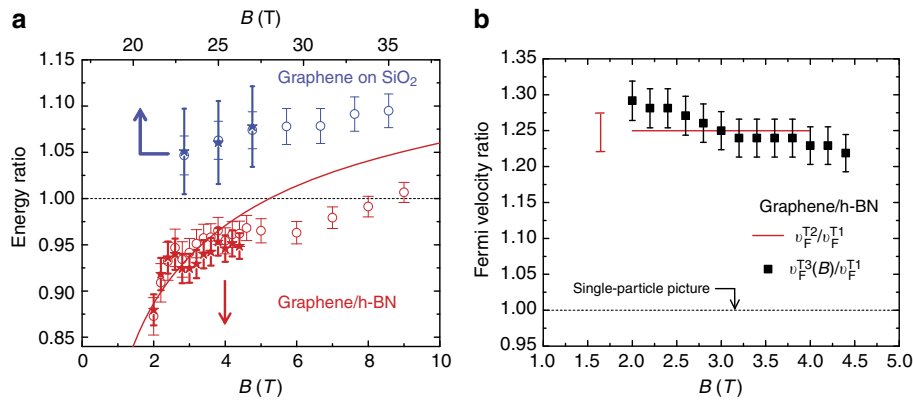

Figure 4 | Many-body effects on LL transitions for pristine and gapped graphene. (**a**) Energy ratios of different LL transitions for graphene on SiO$_2$ (blue colour) and graphene/h-BN sample 1 (red colour) shown in a common vertical scale. Open symbols: $E_{T_2}/[(\sqrt{2}+1)E_{T_1}]$. Solid symbols: $E_{T_3}/[(\sqrt{3}+\sqrt{2})E_{T_1}]$. Red solid line: theoretical result of $E_{T_2}/[(\sqrt{2}+1)E_{T_1}]$ based on equations (3) and (4) for gapped graphene. The ratios for graphene on SiO$_2$ are >1, which is a signature of interaction effects in pristine graphene (Supplementary Note 5). On the other hand, the ratios for graphene/h-BN exhibit an entirely different behaviour, which is consistent with gapped graphene. The error bars of energy ratios are calculated using standard formulas for propagation of uncertainty for division based on the uncertainty in determining the energy of each LL transition from the $T(B)/T(B_0)$ spectra. (**b**) Fermi velocity ratios of different LL transitions for graphene/h-BN with a constant $v_F^{T_1} \approx (0.96 \pm 0.02) \times 10^6$ m s^{-1}. For T_2 transition, a constant Fermi velocity $v_F^{T_2} \approx (1.20 \pm 0.01) \times 10^6$ m s^{-1} is extracted from the data. These ratios are distinct from the value expected from the single-particle picture, which is indicative of interaction effects in gapped graphene. The error bars indicate the range of Fermi velocity values that could fit the data in Fig. 3 (Supplementary Note 4).

T_2, LL$_{-2} \rightarrow$ LL$_{+1}$ and LL$_{-1} \rightarrow$ LL$_{+2}$; T_3, LL$_{-3} \rightarrow$ LL$_{+2}$ and LL$_{-2} \rightarrow$ LL$_{+3}$. Their energies are described by:

$$E_{T_2} = \sqrt{2e\hbar v_F^2 B + (\Delta/2)^2} + \sqrt{(2e\hbar v_F^2 B) \times 2 + (\Delta/2)^2} \quad (4)$$

$$E_{T_3} = \sqrt{(2e\hbar v_F^2 B) \times 2 + (\Delta/2)^2} + \sqrt{(2e\hbar v_F^2 B) \times 3 + (\Delta/2)^2} \quad (5)$$

The energies of T_2 transition show a deviation from linear $\sqrt{B}$ dependence above 4 T (or 220 meV in energy) as shown in Fig. 3, with E^2 deviating from a linear B-dependence, which is perhaps due to the effect of moiré superlattice or many-body interactions. Therefore, we focus on the low field (<4 T) region where the T_2 transition exhibits an overall linear $\sqrt{B}$ dependence, which most likely arises from the intrinsic behaviours of gapped

graphene alone. We observed a splitting of the T_2 transition near 169 meV owing to the coupling to the IR active phonon of h-BN, which nonetheless does not affect the main conclusions of our analysis because this effect only occurs in a very narrow field and energy range. Based on equation (4), we find that the T_2 transition in low field is consistent with a bandgap similar to that extracted from the T_1 transition, $\Delta \approx 38 \pm 4$ meV, and an effective Fermi velocity $v_F^{T_2} \approx (1.20 \pm 0.01) \times 10^6$ m s^{-1} (Supplementary Fig. 4 and Supplementary Note 4). The T_3 transition is discussed in details below and in Supplementary Fig. 5 and Supplementary Note 4.

Comparison with pristine and gapped graphene. We stress that our data on graphene/h-BN cannot be explained by many-body effects of pristine graphene (Supplementary Fig. 6 and

Supplementary Note 5). One prominent feature of interaction effects in pristine graphene is that the effective Fermi velocity varies for different LL transitions, so that the energy ratios $E_{T_2}/[(\sqrt{2}+1)E_{T_1}]$ and $E_{T_3}/[(\sqrt{3}+\sqrt{2})E_{T_1}]$ are higher than one, as demonstrated by previous IR studies[29] and our data on graphene on SiO$_2$. However, the data for graphene/h-BN exhibit an entirely different behaviour (Fig. 4a) compared with interaction effects in pristine graphene. Instead, the energy ratios of different LL transitions for graphene/h-BN are consistent with the behaviours of gapped graphene. A theoretical result of $E_{T_2}/[(\sqrt{2}+1)E_{T_1}]$ based on equations (3) and (4) is shown in Fig. 4a, with $\Delta \approx 38$ meV, $v_F^{T_1} = 0.96 \times 10^6$ m s^{-1} and $v_F^{T_2} = 1.20 \times 10^6$ m s^{-1}, which agrees very well with the experimental results.

Discussion

Previous transport measurements on graphene/h-BN heterostructures indicated a gap of ~ 300 K at 0.4° crystallographic rotational angle (θ)[11]. A recent study[13] reported the existence of large domains of graphene with the same lattice constant as h-BN separated by domain walls with concentrated strain for small θ, and a gap of 360 K was found for $\theta = 0°$. Our optical study provides a direct spectroscopic determination of the bandgap with similar magnitude (~ 440 K) in epitaxial graphene/h-BN heterostructures. This bandgap value is larger than those found in theories within the single-particle picture[18–20], which suggests the relevance of many-body interactions in generating the gap[15,16]. It was argued that the gap at the Dirac point is greatly enhanced by interaction effects due to coupling to a constant sublattice-asymmetric superlattice potential[15], which is not affected by the spatial variations shown in Fig. 1b. The intrinsic gap value for graphene/h-BN obtained in our study provides a critical input for the basic understanding of the gap in this system.

Our study further reveals the crucial role of many-body interactions in renormalizing LL transitions[32] in graphene/h-BN heterostructures. Specifically, the effective Fermi velocity associated with the LL transitions varies with particular transitions as well as the magnetic field. We find that the T$_3$ transition cannot be consistently fitted by equation (5) using a constant v_F, so we use an effective field-dependent parameter $v_F^{T_3}(B)$ to describe this transition (Supplementary Note 4). Figure 4b depicts the Fermi velocity ratios $v_F^{T_2}/v_F^{T_1}$ and $v_F^{T_3}(B)/v_F^{T_1}$, both of which are higher than one and therefore very different from the constant v_F for all transitions expected from single-particle pictures. Intriguingly, $v_F^{T_3}(B)/v_F^{T_1}$ shows a systematic increase in low magnetic fields. For T$_2$ transitions (consider LL$_{-1} \rightarrow$ LL$_{+2}$, for example), it shows $v_F^{T_2} \sim 1.20 \times 10^6$ m s^{-1} even at 1 T field with $E_{T_2} = 115$ meV (Supplementary Fig. 1c), which corresponds to $E_{LL+2} \sim 66$ meV and $E_{LL-1} \sim 49$ meV. According to theoretical studies[33], the band structure of graphene/BN at such low energy scales are quite linear and not strongly modified by the superlattice Dirac points (~ 200 meV; refs 9–12), so the value $v_F^{T_2} \sim 1.20 \times 10^6$ m s^{-1} extracted from data at low magnetic field (thus low energy) is little affected by the superlattice Dirac points. Similar argument can be made for T$_1$ and T$_3$ transitions at low magnetic fields and low energy. Note that the LL transitions at high field and high energy (for instance, T$_2$ transition above 4 T field) may be affected by the band structure modification due to the superlattice Dirac points[8,33], but our discussions here are only focused on the low field regime shown in Fig. 4b. Our results in Fig. 4b indicate LL renormalization due to many-body interactions in magnetic field. Theoretical studies[34–37] showed that interaction effects of electron-hole excitations between LLs, such as direct Coulomb interactions between the excited electrons and holes and the exchange self-energy of electrons and holes between LLs, can significantly renormalize the inter-LL transition

energy. The observation shown in Fig. 4b in gapped graphene is qualitatively similar to the results from many-body theories[34–37] as well as experimental studies[29] on pristine graphene, so our results strongly suggest contributions of many-body effects to the inter-LL transitions[34–37]. Further theoretical investigations are required to quantitatively understand these interactions in gapped graphene, with many open questions yet to be addressed such as the role of superlattice potential[15] and bond distortion[20] in graphene/h-BN heterostructures.

Multi-valley (band extrema in momentum space) Dirac systems such as gapped graphene, silicene and 2D transition metal dichalcogenides are described by the same Dirac Hamiltonian and share several essential properties such as valley-dependent orbital magnetic moment and Berry curvature[23,38], which are intimately related to their unconventional valley-dependent LL structures[38–40]. In this context, the strong LL renormalization observed here has broad implications for fundamental studies of many novel phenomena related to LLs in these Dirac materials, such as magnetic control of valley degree of freedom[38] and valley-spin polarized magneto-optical response[39,40].

In summary, we have observed a bandgap of ~ 38 meV (440 K) in graphene/h-BN heterostructures with zero crystallographic rotation angle using magneto-optical spectroscopy. The intrinsic gap value reported here is important for fundamental understanding of the bandgap and many-body interaction effects in this system. Our demonstration of a finite bandgap in epitaxial graphene/h-BN heterostructures can also lead to novel applications in electronics and optoelectronics.

Methods

Sample preparation and characterization. h-BN was mechanically exfoliated onto double-side-polished SiO$_2$/Si substrates with 300 nm SiO$_2$. Graphene was epitaxially grown on h-BN by remote plasma enhanced chemical vapour deposition[12]. Some multilayer grains can be found on monolayer graphene in as-grown samples, so hydrogen plasma etching technique[12] was applied to reduce these additional grains. The resulting sample is continuous monolayer graphene with minor etched hexagonal pitches in plane, as shown in Fig. 1c. The moiré pattern (Fig. 1c) due to lattice mismatch shows a periodicity of 15 ± 1 nm as measured by atomic force microscopy, indicating zero crystallographic alignment angle between graphene and h-BN[12]. This moiré pattern is observed over the entire areas of all samples, establishing these epitaxial samples as single-crystalline and single-domain graphene heterostructures. The samples studied in this work have typical lateral sizes of ~ 100 μm. The observed sharp LL transitions indicate that the optical absorption of our samples is little affected by defects or grain boundaries. The effective mobility of our samples estimated from the widths of the resonances in the optical spectra is higher than 50,000 cm^2 V^{-1} s^{-1} (Supplementary Fig. 3 and Supplementary Note 2). The absence of the LL$_{-1} \rightarrow$ LL$_{-0}$ and LL$_{+0} \rightarrow$ LL$_{+1}$ transitions in our optical data indicates that the Fermi energy is within the gap for our samples, namely $E_F < 19$ meV (Supplementary Note 3).

Magneto-transmission measurements. The measurements were performed at ~ 4.5 K in a superconducting or resistive magnet in the Faraday geometry (magnetic field perpendicular to the sample surface). IR light from a Fourier transform spectrometer is delivered to the sample using a copper light pipe, and the light transmitted through the sample is detected by a composite Si bolometer. The focus of the IR light on the sample is $\sim 0.5–1$ mm. To reduce the stray light around our small samples, an aluminium aperture of ~ 200 μm diameter was placed around the sample. We report data at energies above 60 meV corresponding to wavelengths shorter than 20 μm, which ensures that the wavelength is significantly smaller than the sizes of the samples, and therefore a macroscopic description of the data using optical constants is applicable.

References

1. Dean, C. R. et al. Boron nitride substrates for high-quality graphene electronics. Nat. Nanotech. **5,** 722–726 (2010).
2. Geim, A. K. & Grigorieva, I. V. Van der Waals heterostructures. Nature **499,** 419–425 (2013).
3. Britnell, L. et al. Field-effect tunneling transistor based on vertical graphene heterostructures. Science **335,** 947–950 (2012).

4. Choi, M. S. et al. Controlled charge trapping by molybdenum disulphide and graphene in ultrathin heterostructured memory devices. Nat. Commun. 4, 1624 (2013).

5. Britnell, L. et al. Strong light - matter interactions in heterostructures of atomically thin films. Science 340, 1311–1314 (2013).

6. Roy, K. et al. Graphene–MoS2 hybrid structures for multifunctional photoresponsive memory devices. Nat. Nanotech. 8, 826–830 (2013).

7. Yu, W. J. et al. Vertically stacked multi-heterostructures of layered materials for logic transistors and complementary inverters. Nat. Mater. 12, 246–252 (2013).

8. Yankowitz, M. et al. Emergence of superlattice Dirac points in graphene on hexagonal boron nitride. Nat. Phys. 8, 382–386 (2012).

9. Ponomarenko, L. A. et al. Cloning of Dirac fermions in graphene superlattices. Nature 497, 594–597 (2013).

10. Dean, C. R. et al. Hofstadter's butterfly and the fractal quantum Hall effect in moiré superlattices. Nature 497, 598–602 (2013).

11. Hunt, B. et al. Massive Dirac fermions and Hofstadter butterfly in a van der Waals heterostructure. Science 340, 1427–1430 (2013).

12. Yang, W. et al. Epitaxial growth of single-domain graphene on hexagonal boron nitride. Nat. Mater. 12, 792–799 (2013).

13. Woods, C. R. et al. Commensurate-incommensurate transition for graphene on hexagonal boron nitride. Nat. Phys 10, 451–456 (2014).

14. Park, C.-H., Yang, L., Son, Y.-W., Cohen, M. L. & Louie, S. G. New generation of massless Dirac fermions in graphene under external periodic potentials. Phys. Rev. Lett. 101, 126804 (2008).

15. Song, J. C. W., Shytov, A. V. & Levitov, L. S. Electron interactions and gap opening in graphene superlattices. Phys. Rev. Lett. 111, 266801 (2013).

16. Bokdam, M., Amlaki, T., Brocks, G. & Kelly, P. J. Band gaps in incommensurable graphene on hexagonal boron nitride. Phys. Rev. B. 89, 201404 (2014).

17. Giovannetti, G., Khomyakov, P. A., Brocks, G., Kelly, P. J. & van den Brink, J. Substrate-induced band gap in graphene on hexagonal boron nitride: Ab initio density functional calculations. Phys. Rev. B 76, 073103 (2007).

18. Sachs, B., Wehling, T. O., Katsnelson, M. I. & Lichtenstein, A. I. Adhesion and electronic structure of graphene on hexagonal boron nitride substrates. Phys. Rev. B 84, 195414 (2011).

19. Kindermann, M., Uchoa, B. & Miller, D. L. Zero-energy modes and gate-tunable gap in graphene on hexagonal boron nitride. Phys. Rev. B 86, 115415 (2012).

20. Jung, J., DaSilva, A., Adam, S. & MacDonald, A. H. Origin of band gaps in graphene on hexagonal boron nitride. Preprint at http://arxiv.org/abs/1403.0496 (2014).

21. Yao, W., Yang, S. A. & Niu, Q. Edge states in graphene: From gapped flat-band to gapless chiral modes. Phys. Rev. Lett. 102, 096801 (2009).

22. Semenoff, G. W., Semenoff, V. & Zhou, F. Domain walls in gapped graphene. Phys. Rev. Lett. 101, 087204 (2008).

23. Xiao, D., Yao, W. & Niu, Q. Valley-contrasting physics in graphene: magnetic moment and topological transport. Phys. Rev. Lett. 99, 236809 (2007).

24. Yao, W., Xiao, D. & Niu, Q. Valley-dependent optoelectronics from inversion symmetry breaking. Phys. Rev. B 77, 235406 (2008).

25. Novoselov, K. S. et al. A roadmap for graphene. Nature 490, 192–200 (2012).

26. Mott, N. F. & Davis, E. A. Electronic Processes in Non-Crystalline Materials 2nd edn (Clarendon Press, 1979).

27. von Klitzing, K. The quantized Hall effect. Rev. Mod. Phys. 58, 519–531 (1986).

28. Chen, X. et al. Dirac edges of fractal magnetic minibands in graphene with hexagonal moiré superlattices. Phys. Rev. B 89, 075401 (2014).

29. Jiang, Z. et al. Infrared spectroscopy of Landau levels of graphene. Phys. Rev. Lett. 98, 197403 (2007).

30. Sadowski, M. L., Martinez, G., Potemski, M., Berger, C. & de Heer, W. A. Landau Level Spectroscopy of Ultrathin Graphite Layers. Phys. Rev. Lett. 97, 266405 (2006).

31. Gusynin, V. P., Sharapov, S. G. & Carbotte, J. P. Magneto-optical conductivity in graphene. J. Phys. Condens. Matter. 19, 026222 (2007).

32. Goerbig, M. O. Electronic properties of graphene in a strong magnetic field. Rev. Mod. Phys. 83, 1193–1243 (2011).

33. Wallbank, J. R., Patel, A. A., Mucha-Kruczynski, M., Geim, A. K. & Fal'ko, V. I. Generic miniband structure of graphene on a hexagonal substrate. Phys. Rev. B 87, 245408 (2013).

34. Iyengar, A., Wang, J., Fertig, H. A. & Brey, L. Excitations from filled Landau levels in graphene. Phys. Rev. B 75, 125430 (2007).

35. Bychkov, Y. A. & Martinez, G. Magnetoplasmon excitations in graphene for filling factors ν≤6. Phys. Rev. B 77, 125417 (2008).

36. Roldán, R., Fuchs, J. N. & Goerbig, M. O. Spin-flip excitations, spin waves, and magnetoexcitons in graphene Landau levels at integer filling factors. Phys. Rev. B 82, 205418 (2010).

37. Shizuya, K. Many-body corrections to cyclotron resonance in monolayer and bilayer graphene. Phys. Rev. B 81, 075407 (2010).

38. Cai, T. et al. Magnetic control of the valley degree of freedom of massive Dirac fermions with application to transition metal dichalcogenides. Phys. Rev. B 88, 115140 (2013).

39. Tabert, C. J. & Nicol, E. J. Valley-spin polarization in the magneto-optical response of silicene and other similar 2D crystals. Phys. Rev. Lett. 110, 197402 (2013).

40. Rose, F., Goerbig, M. O. & Piéchon, F. Spin- and valley-dependent magneto-optical properties of MoS2. Phys. Rev. B 88, 125438 (2013).

Author contributions

Z.-G.C. and Z.S. initiated the optical studies; Z.-G.C. carried out the optical experiments; Z.S. and Y.L. participated in part of the measurements; W.Y. and X.L. grew and characterized the graphene/h-BN samples; H.Y. provided the graphene on SiO₂ samples; F.W., G.Z. and Z.L. supervised the project; Z.-G.C. and Z.L. analysed the data and wrote the manuscript. All authors discussed the results and commented on the paper.

Additional information

Supplementary Information accompanies this paper at http://www.nature.com/naturecommunications

Competing financial interests: The authors declare no competing financial interests.

Reprints and permission information is available online at http://npg.nature.com/reprintsandpermissions/

How to cite this article: Chen, Z.-G. et al. Observation of an intrinsic bandgap and Landau level renormalization in graphene/boron-nitride heterostructures. Nat. Commun. 5:4461 doi: 10.1038/ncomms5461 (2014).